Liu *et al. Energy Mater.* **2025**, *5*, 500054
DOI: 10.20517/energymater.2024.69

Energy Materials

Article

Open Access

Check for updates

In-situ study of lithium insertion on the electrochemical-mechanical coupling behavior of graphite composite electrodes

Jiahui Liu[1], Honghui Gu[2,3], Hainan Jiang[1], Chenhao Shen[1], Yi Yao[1], Kai Shen[1], Yuejiu Zheng[1], Dawei Li[1,*]

[1]School of Mechanical Engineering, University of Shanghai for Science and Technology, Shanghai 200093, China.
[2]Jiangsu Key Laboratory of Materials and Technologies for Energy Storage, College of Materials Science and Technology, Nanjing University of Aeronautics and Astronautics, Nanjing 210016, Jiangsu, China.
[3]State Key Laboratory of Space Power Sources, Shanghai Institute of Space Power-Sources, Shanghai 200245, China.

***Correspondence to:** Prof./Dr. Dawei Li, School of Mechanical Engineering, University of Shanghai for Science and Technology, 580 Jungong Road, Shanghai 200093, China. E-mail: lidawei@usst.edu.cn

How to cite this article: Liu, J.; Gu, H.; Jiang, H.; Shen, C.; Yao, Y.; Shen, K.; Zheng, Y.; Li, D. *In-situ* study of lithium insertion on the electrochemical-mechanical coupling behavior of graphite composite electrodes. *Energy Mater.* **2025**, *5*, 500054. https://dx.doi.org/10.20517/energymater.2024.69

Received: 7 Jul 2024 **First Decision:** 30 Jul 2024 **Revised:** 30 Aug 2024 **Accepted:** 30 Sep 2024 **Published:** 25 Feb 2025

Academic Editor: Chunhui Duan **Copy Editor:** Fangling Lan **Production Editor:** Fangling Lan

Abstract

Graphite has long served as one of the most commonly used anode materials in lithium-ion batteries, where its electrochemical-mechanical coupling performance is critical for maintaining structural stability and extending cycle life. This study investigates the evolution of the electrochemical-mechanical coupling characteristics of graphite electrodes during electrochemical cycling. Experiments were performed using *in situ* curvature testing, combined with *in situ* X-ray Diffraction analysis. A physical model was created to analyze the variations in curvature, Young's modulus, strain, and partial molar volume of the graphite composite electrodes. The results indicate that the modulus of elasticity augments with the concentration of lithium ions during lithiation. Additionally, the partial molar volume undergoes periodic changes with the state of charge. *In-situ* X-ray Diffraction experiments revealed the lithiation phase transformation process in graphite. The interlayer spacing was calculated by tracking the evolution of the (001) and (002) diffraction peaks, which verified the accuracy of the partial molar volume during the electrochemical cycle. This further elucidates the phase transformation mechanisms of lithium intercalation and the volumetric changes of the active material within the graphite anode.

Keywords: Modulus, partial molar volume, *in situ* measurements, graphite composite electrode, lithium batteries

INTRODUCTION

As the global demand for clean energy and electric vehicles continually increases, the lithium battery industry is experiencing rapid growth[1-3]. Graphite is chosen as the anode material for lithium batteries based on its stable performance, low-voltage platform, and cost-effectiveness[4-6]. During the electrochemical reaction, the (de)intercalation of lithium ions results in alterations to the interlayer spacing of graphite, leading to volume expansion and contraction[7-10]. At the same time, this process is constrained by the metal current collector, which causes the electrodes to deform and induces stress. The bilayer electrodes can result in the bending curvature, while the batteries can lead to volume expansion[11,12]. The stress generated by diffusion subsequently causes cracks, delamination, and other damage in the electrode, adversely affecting the capacity density and cycle life of lithium batteries[13-15].

Thus, the measurement method and mathematical need to be developed to get a deep understanding of the working mechanism of the battery electrodes. Here, real-time monitoring of the mechanical characteristics of composite electrodes during electrochemical reactions through *in-situ* experiments can significantly enhance our understanding of commercial lithium batteries. Additionally, an in-depth investigation of the mechanical-electrochemical coupling performance evolution during cycling can guide the design of high-capacity commercial lithium batteries. *In-situ* measurement techniques can accurately capture the stress, strain, and damage degree of lithium battery electrodes during electrochemical reactions, providing a deeper understanding of the mechanisms affecting their capacity density and cycle life[16-19]. Existing research has developed *in-situ* measurement methods to explore the electrochemical-mechanical coupling mechanisms of lithium battery electrodes[20-23]. For instance, digital image correlation (DIC) was utilized to investigate the mechanical evolution of graphite anode during lithiation and delithiation, demonstrating that strain evolves with changes in the electrode surface morphology[24,25]. *In situ* Raman spectroscopy experiments were proposed to analyze and discuss deformation mechanisms and rate response characteristics, quantifying the micro-deformation evolution of graphite anodes at various charge-discharge rates[26]. DIC was combined with a custom-designed device to measure the strain of graphite electrodes *in situ* during electrochemical cycling. As lithium ions intercalate, graphite undergoes a series of phase transformations, forming interlayer compounds (Li_XC_6)[27]. Neutron diffraction was utilized to observe phase transitions in graphite electrodes during cycling, thereby revealing the presence and evolution of phases such as LiC_{12} and LiC_6[28]. During the cycling of graphite electrodes, the voltage exhibits characteristic lithium-ion (de)intercalation plateaus[29]. Studies have shown that different phases within the graphite electrode, referred to as stages, are defined based on the concentration of lithium ions in the graphite[30-32]. The diffusivity of lithium ions and the mechanical properties of the lithiation products are contingent upon the lithium concentration[33-35]. This dependency results in the stage-specific material characteristics observed in graphite electrodes. Thus, understanding the behavior and material properties of graphite electrodes at varying lithium concentrations is crucial for optimizing their electrochemical performance[36].

Raman spectroscopy detects carbon-carbon vibrational modes in graphite, providing insights into lithium intercalation by altering the D and G band positions and intensities[37]. However, its effectiveness is limited by laser wavelength, potentially leading to localized, unrepresentative analysis. In contrast, Nuclear magnetic resonance (NMR) spectroscopy probes the local lithium environment within graphite, identifying ion positions and distribution, although the signal strength is dependent on lithium concentration[38]. Transmission electron microscopy (TEM) offers direct visualization of the graphite structure post-intercalation, but the technique is hindered by complex sample preparation and the risk of sample damage[39]. X-ray diffraction (XRD) is widely used to examine the crystalline changes in layered anode materials during electrochemical cycling[40-42]. *In-situ* XRD and *in-situ* pressure analysis techniques were employed to monitor the structural and volume changes of graphite anodes during charge and discharge,

demonstrating that incomplete lithiation can induce significant lattice strain[43]. Systematic *in-situ* XRD studies were used to investigate the structural alterations of graphite-silicon electrodes compared to pristine graphite during cycling, indirectly exploring structural changes through crystallographic variations of the included graphite[44].

This study employs two *in-situ* measurement methods to analyze the volume expansion and structural alterations of graphite electrodes during electrochemical cycling. The study employs an integrated approach using *in-situ* XRD to examine microstructural changes in the crystal structure under different electrochemical states. Simultaneously, *in-situ* curvature testing is used to evaluate the macroscopic mechanical stability of the electrodes during the electrochemical process. This combined methodology, linking microstructural insights from XRD with macroscopic curvature observations, provides a comprehensive perspective on the electrode behavior, effectively bridging the gap between micro- and macro-scale analyses. By combining these methods, the study monitors and analyzes the evolution of partial molar volume and modulus during lithiation, providing a comprehensive understanding of the phase transitions in graphite materials. This integrated approach enables a detailed examination of macroscopic curvature phenomena from a microscopic perspective, revealing crystal structure changes by XRD and assessing the mechanical stability of electrodes by the *in-situ* curvature mechanics testing during electrochemical processes.

EXPERIMENTAL

Electrode preparation

The graphite composite electrodes were prepared by mixing powders of graphite, conductive carbon black, and carboxymethyl cellulose (CMC) (90:2.5:7.5) in deionized water. The well-mixed slurry was then uniformly coated onto copper foil of two different thicknesses and roll-pressed. The electrodes were dried for ten hours in a vacuum environment at 110 °C. The volume fractions of each component were determined based on their respective volumes, calculated as the ratio of mass to density. Consequently, the active layer exhibited a porosity of approximately 59.62%, with the active material accounting for around 35.32% of the total volume using Supplementary Equations 1 and 2. The thickness of the active layer was measured to be 40 μm. The thicknesses of the current collectors were 10 and 22 μm, respectively, and their Young's modulus was determined by dynamic mechanical analysis (DMA) tensile tests to be roughly 55 and 36.9 GPa. The detailed DMA curves are provided in Supplementary Figure 1 and Supplementary Table 1 of the Supplementary Materials. Figure 1A illustrates the initial state of the electrode structure as observed via scanning electron microscopy (SEM). Figure 1B presents the energy-dispersive X-ray spectroscopy (EDS) spectrum of the electrode. The detected weight percentage of the carbon element in the graphite composite electrode was 97%, confirming the successful fabrication of the electrode.

Model cell assembly

The model cells were assembled in a glove box (O_2, H_2O ≤ 0.1 ppm). A microporous polypropylene membrane (20 μm, Celgard 2500) was used as a separator between the graphite anode and lithium metal to prevent short circuits. The model cells were constructed with a quartz window of sufficient transparency to permit real-time monitoring of the bending deformation of the graphite composite electrode. The graphite composite electrode was constructed in a cantilever structure (15 mm × 3 mm). Figure 2 shows the *in-situ* curvature testing system and a schematic of the bending deformation of the graphite composite electrode. The electro-mechanical coupling measurements were done with the model cell using lithium metal as the cathode. The electrolyte utilized was a solution of 1M $LiPF_6$, prepared in a 1:1 vol% ratio of ethylene carbonate and diethyl carbonate (EC:DEC) and provided by Nanjing Jiangshan Energy Technology Co., Ltd. The prepared model cells were left to stand in a glove box for 12 h to ensure thorough wetting.

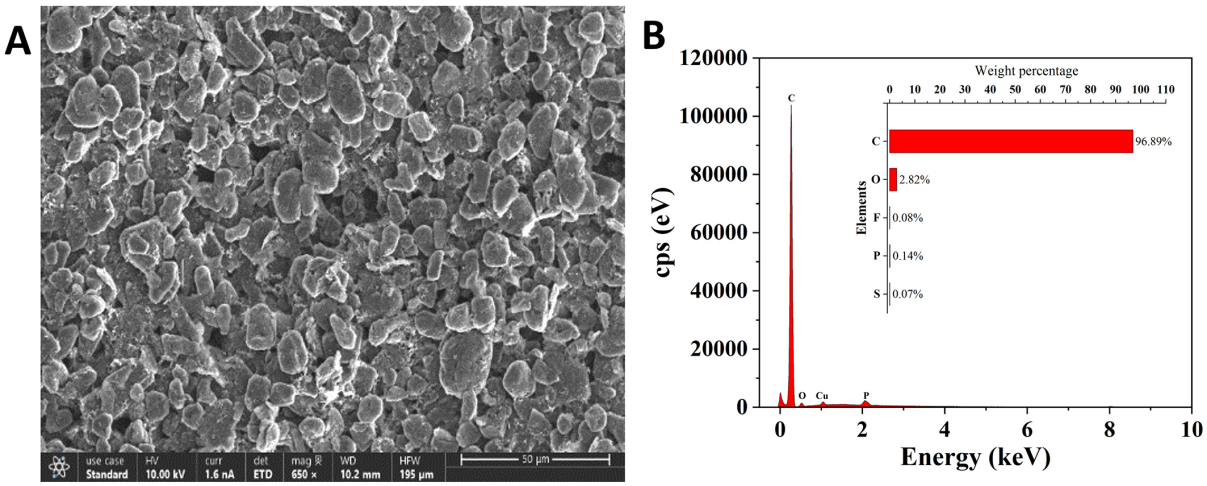

Figure 1. (A) SEM image and (B) EDS spectra of the graphite electrode.

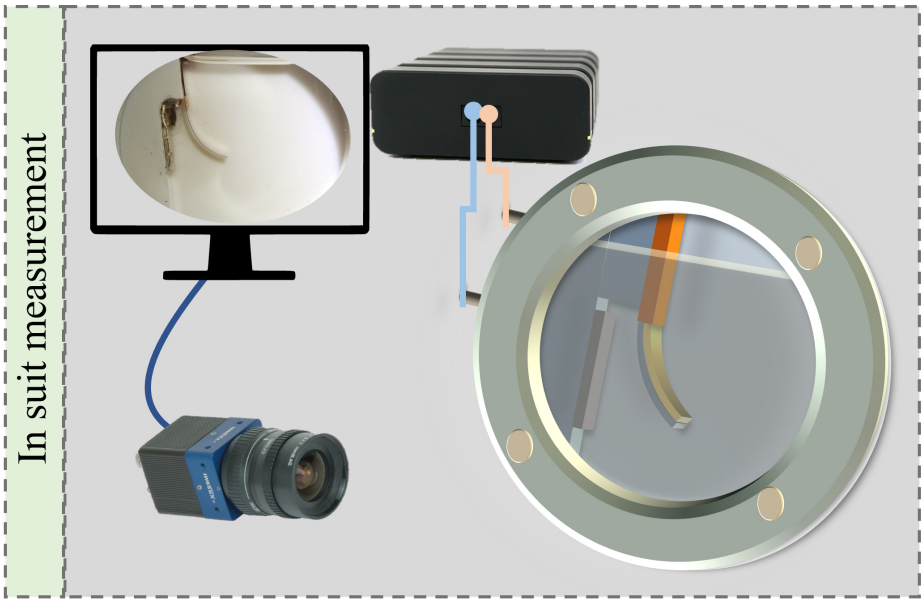

Figure 2. Schematic illustration of the *in-situ* curvature testing system.

Electrochemical testing

All electrochemical measurements were performed at room temperature utilizing a CT-4000 mA battery testing system produced by NEWARE. In the lithium battery testing system, the rate of cell cycle progression is set up to be 1/10C at a current density of 108.89 μA/cm^2, with voltage limits set at 0.1 and 1.2 V. A 3-min rest step was included after each charge-discharge cycle. A relatively low charge-discharge rate was chosen to maintain uniform lithium-ion intercalation in the active layer, as lowering the charge rate helps reduce polarization effects on the graphite electrode during cycling. The bending deformation of the graphite composite electrode was recorded in real time during electrochemical cycling using an industrial CCD camera (CM200GE). Images were captured by the CCD camera every 2 min. Electrochemical parameters such as voltage, current, time, and capacity were recorded by the battery testing system at a frequency of 1 Hz.

XRD spectra were collected using a PANalytical Empyrean diffractometer with Mo target radiation. *In-situ* XRD analysis was conducted on the graphite composite electrode from 0% state of charge (SOC) to 100% SOC, using a conventional small-angle scan with a scan rate of 0.02°/min and a scan range of 3° to 60°, focusing on the anode active material range of 10° to 13°. Combined with *in-situ* curvature measurements, the volume changes of graphite during different stages of lithiation were studied.

Analysis of curvature change mechanism

As shown in Figure 3A and B, the curvature of composite graphite electrodes with two thicknesses of current collectors during cycling. Therefore, we created a schematic of a cantilever double-layer electrode with lithium intercalation based on the model cells. As shown in Figure 3C, the thickness of the current collector is denoted as h_c, and that of the active layer is h_a. During electrochemical cycling, the intercalation and de-intercalation of lithium ions cause the active layer of the composite electrode to undergo expansion and contraction. Nevertheless, the active layer is constrained by the current collector, which results in a strain mismatch that gives rise to the bending deformation of the electrode[45]. In this work, the electrodes were ensured to deform within the elastic range without any plastic deformation effects. The deformation of the electrode was continuously monitored in real-time by a CCD camera throughout the electrochemical cycling process. The curvature was analyzed to obtain the mechanical parameters of electrodes during the electrochemical cycling process, which is acquired using image analysis.

According to the theory of small deformations, the in-plane strain in the direction of the x-axis can be given as:

$$\varepsilon = \varepsilon_0 + z\kappa \tag{1}$$

where ε_0 is the in-plane strain on the $z = 0$ plane, representing the electrode strain, and κ is the curvature. To facilitate calculation and analysis, this study assumes that the complex structure of the active layer is completely elastic and macroscopically isotropic. Therefore, the constitutive relationships for the active layer and current collector can be written as:

$$\sigma_a = E_1(\varepsilon_0 + z\kappa) - 1/3 \times E_1\Omega c,\ \sigma_c = E_c(\varepsilon_0 + z\kappa) \tag{2}$$

where E_1 represents the Young's modulus of the electrode's active layer, and E_c represents the Young's modulus of the copper foil. Ω indicates the molar volume change. σ_c and σ_a represent the stress in the current collector and active layer, respectively. The Young's modulus of the electrode's active layer depends on the lithium-ion concentration. Nevertheless, given the relatively low charge rate during electrochemical cycling, it can be assumed that the concentration gradient in the thickness direction is negligible; Consequently, both the concentration and Young's modulus of the active layer are presumed to remain constant.

The electrode's boundary constraints are as follows:

$$\int_z \sigma_x dz = 0 \tag{3}$$

$$\int_z \sigma_x z dz = 0 \tag{4}$$

Solving Equations (2) and (3) simultaneously:

$$\varepsilon_0 = \frac{\Omega c(E_1^2 h_a^4 + 3E_c E_1 h_c^2 h_a^2 + 4E_c E_1 h_c^3 h_a)}{3(E_1^2 h_a^4 + 4E_c E_1 h_a^3 h_c + 6E_c E_1 h_c^2 h_a^2 + 4E_c E_1 h_c^3 h_a + E_c^2 h_c^4)} \quad (5)$$

Combining Equations (2), (4), and (5):

$$\kappa h_a R_h^4 R_E^2 + (4\kappa h_a R_h + 6\kappa h_a R_h^2 + 4\kappa h_a R_h^3 - 2\Omega_C R_h - 2\Omega_C R_h^2) R_E + \kappa h_a = 0 \quad (6)$$

where h_a and h_c are the thicknesses of the active layer and copper foil, respectively. To ensure consistency, the thickness h_a of the active layers in all electrodes was controlled to be the same, denoted as h_1. $R_h = h_c/h_1$ and $R_E = E_c/E_1$ represent the thickness ratio and modulus ratio, respectively. The curvature of the two electrodes can be expressed as h_{c1}, $E_{c1,\ \kappa 1}$, h_{c2}, $E_{c2,\ \kappa 2}$.

$$\begin{aligned} &\kappa_1 h_1 E_1^2 + \kappa_1 h_1 (h_{c1}/h_1)^4 E_{C1}^2 \\ &+2\left\{\kappa_1 h_1 [2(h_{c1}/h_1) + 3(h_{c1}/h_1)^2 + 2(h_{c1}/h_1)^3] - \Omega_C [h_{c1}/h_1 + (h_{c1}/h_1)^2]\right\} E_{C1} E_1 = 0 \end{aligned} \quad (7)$$

$$\begin{aligned} &\kappa_2 h_1 E_1^2 + \kappa_2 h_1 (h_{c2}/h_1)^4 E_{C2}^2 \\ &+2\left\{\kappa_2 h_1 [2(h_{c2}/h_1) + 3(h_{c2}/h_1)^2 + 2(h_{c2}/h_1)^3] - \Omega_C [h_{c2}/h_1 + (h_{c2}/h_1)^2]\right\} E_{C2} E_1 = 0 \end{aligned} \quad (8)$$

Therefore

$$E_1 = \frac{\left[\begin{array}{c} P^2 (W_1 G_2 - W_2 G_1)^2 \\ -4(F_2 - F_1) P W_1 W_2 (Q_1 E_{C2} + Q_2 E_{C1} W_2) \end{array}\right]^{1/2} - P(W_1 G_2 - W_2 G_1)}{2PW_1 W_2 (F_2 - F_1)} \quad (9)$$

Among:

$P = E_{C2} * E_{C1}$

$F_i = \kappa_i h_1 / [E_{Ci}(Rh_i + Rh_i^2)]$ (i = 1,2)

$W_i = (Rh_i + Rh_i^2)$ (i = 1,2)

$G_i = 4\kappa_i h_1 R_{hi} + 6\kappa_i h_1 R_{hi}^2 + 4\kappa_i h_1 R_{hi}^3$ (i = 1,2)

$Q_i = \kappa_i h_1 R h_i^4 E c_i^2$ (i = 1,2)

Further solving gives:

$$\Omega = G_1/2W_1 + (\kappa_1 h_1 E_1^2 + Q_1)/[2E_{c1} E_1 W_1] \quad (10)$$

RESULTS AND DISCUSSION

To better understand the variations in mechanical properties of graphite composite electrodes with current collectors of different thicknesses, this study employed an *in-situ* testing system to measure electrode curvature. The analysis focused on evaluating the mechanical characteristics of the electrodes during cycling.

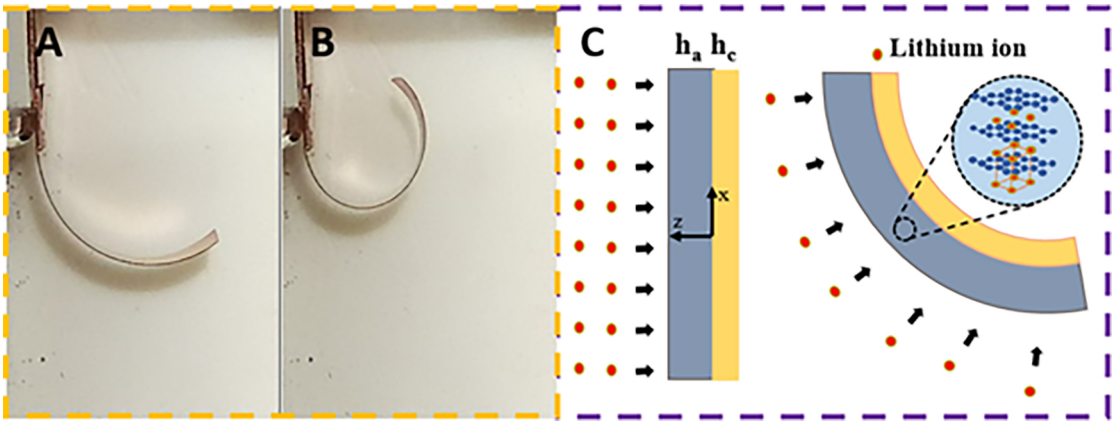

Figure 3. The curvature of graphite electrode corresponding to electrodes in SOC 100% at the end of the third cycle: (A) 22 μm; (B) 10 μm; (C) Mathematical model.

During the discharge process, the graphite particles begin to swell due to the intercalation of Li^+ into the active layer. Meanwhile, the current collector constrains this expansion, resulting in a mismatch that leads to the bending deformation of the electrode. Figure 4A showed the degree of bending deformation of graphite electrodes varies with the SOC. Furthermore, the electrode with a thickness of 10 μm exhibits greater bending deformation during lithiation. Therefore, the thinner the current collector, the greater the mismatch strain, leading to an increase in bending curvature. As shown in Figure 4B, the voltage curves of the two electrodes display comparable patterns, indicating that the reaction behavior is almost identical despite the use of current collectors with different thicknesses. The detailed voltage-capacity curve during cycling is provided in Supplementary Figure 2 of the Supplementary Materials.

The discharge voltage curves of the cycles exhibit the characteristics of typical lithium (de)intercalation plateaus, which correspond to the different stages of graphite lithiation. The existence of various phases is contingent upon the concentration of lithium (i.e., 1L, 4L, 3L, 2L, 2, and 1), as shown in Figure 5. During the lithium intercalation process, a series of voltage plateaus is observed in graphite, which can be attributed to phase transitions. The formation of LiC_{12} and LiC_6 is accompanied by a reduction in voltage, followed by a plateau[46].

In the first two cycles, the formation and evolution of the solid electrolyte interface (SEI) exhibit more complex reaction mechanisms compared to subsequent cycles[47]. To avoid the influence of the SEI film on the electrode's mechanical response, this study mainly analyzed the third electrochemical cycling. To enable clearer observation and analysis, the curvature of the third cycle was normalized. As shown in Figure 5, electrodes with thinner current collectors exhibit a faster rate of curvature. The curvature of the electrodes gradually increases with normalized concentration. The electrode with a 10 μm current collector shows a curvature peak value of 312 m^{-1}, corresponding to 100% SOC, whereas the electrode with a thickness of 22 μm shows a curvature peak value of 165 m^{-1}. Based on the curvature from the third lithiation process, the mechanical properties of the graphite anode were further analyzed.

By substituting the curvature data in the third cycle into Equation (9), the relationship between the modulus and normalized concentration can be determined, as illustrated in Figure 6A. Utilizing the parameters of electrodes in Equation (9), it was found that a current collector thickness of 10 μm corresponds to a

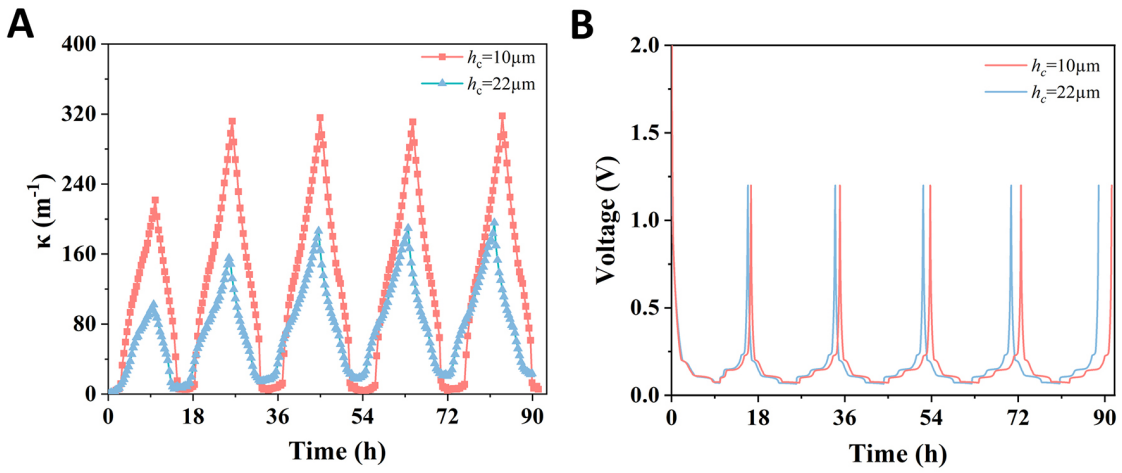

Figure 4. (A) Curvature and (B) voltage evolution of composite graphite electrodes in five cycles.

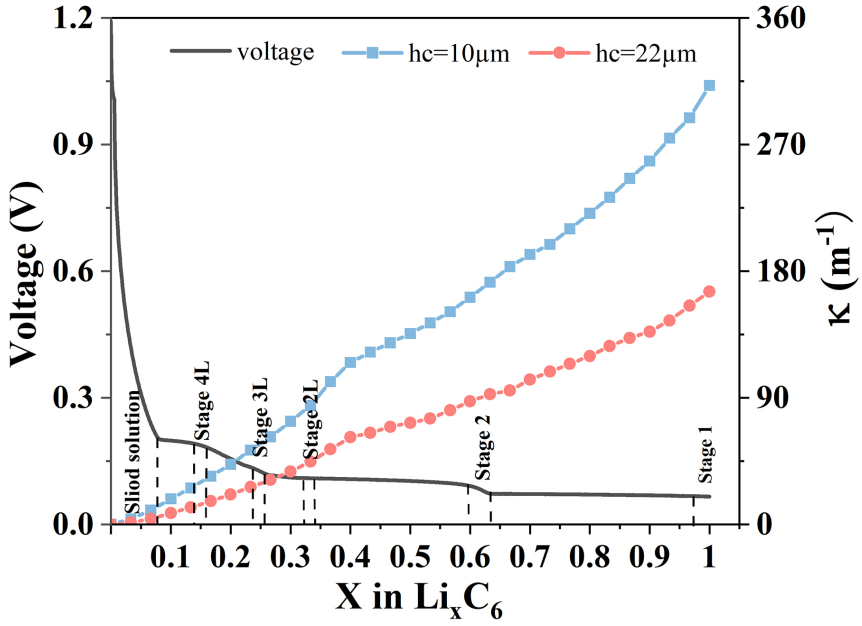

Figure 5. Curvature and voltage evolution of the graphite composite electrodes in the third process of the lithiation cycle.

modulus of 55 GPa, while a thickness of 22 μm corresponds to a modulus of 36.9 GPa. To eliminate the influence of the active layer on the electrode properties, all electrodes were prepared with an active layer thickness of 40 micrometers and an active surface density of 1.097 mAh/mm^2. This was achieved by controlling the graphite electrode active layers to have a consistent thickness and the same volume fraction of active particles during fabrication. This approach allowed for a precise analysis of the mechanical properties, focusing specifically on the influence of the current collector. The modulus changes in the two active layers are shown to be consistent [Figure 6A]. During the lithiation process, the intercalation of lithium ions leads to expansion in the graphite material, altering its mechanical properties and increasing the interatomic forces within the graphite layers. These factors collectively increase the Young's modulus of the active layer as lithiation progresses. As lithiation continues, the active layer gradually hardens. The trend is consistent with the results in previous research[48].

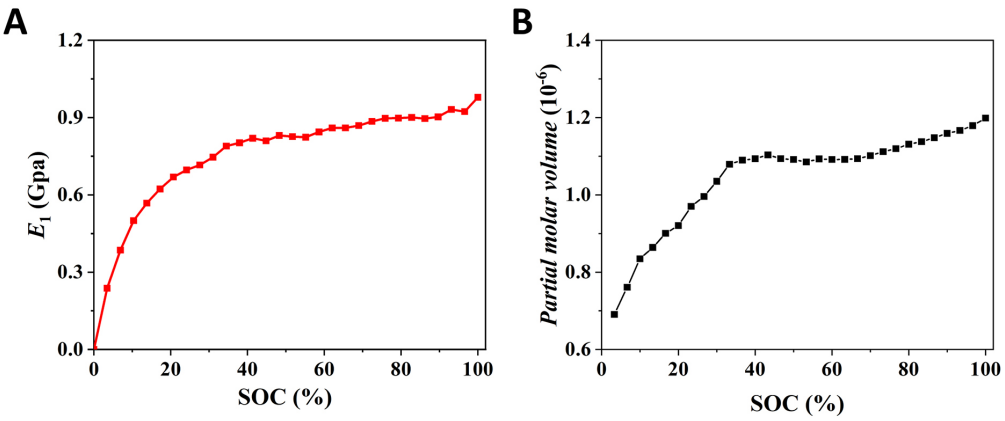

Figure 6. (A) Elastic modulus and (B) partial molar volume evolution of the graphite composite electrodes in the third lithiation.

As the SOC increases, the graphite electrode becomes considerably harder. During the third lithiation process, the elastic modulus of the electrode increases rapidly. The change in partial molar volume can be calculated through Equation (10). As shown in Figure 6B, approximately linear growth in the partial molar volume of the active layer before 30% SOC. However, between 30% and 68% SOC, it stabilizes at a plateau. Beyond 68% SOC up to 100%, the partial molar volume transitions to linear growth.

Under the constraint of the current collector, graphite experiences volume expansion during lithiation, leading to compressive stress within the electrode that escalates with a higher State of Charge (SOC), as shown in Figure 7. The stress on the active layer is influenced by the thickness of the current collector, with thinner collectors applying less compressive stress. Conversely, thicker current collectors impose greater constraints on the expansion of the active layer, reducing deformation and resulting in electrodes with thicker collectors showing smaller curvature. In order to delve deeper into this mechanism, *in-situ* XRD experiments were carried out on the graphite anode.

Figure 8A illustrates the XRD spectroscopy of the graphite electrode. The *in-situ* XRD tests from 0% to 100% SOC clearly show that the position of the graphite (002) diffraction peak shifts continuously towards lower angles, and the diffraction intensity gradually decreases. In the lithiation process, graphite exhibits a sequence of phase transitions, consistent with findings reported in previous studies[49]. The changes from graphite (~12.1°) to other intercalation stages are very apparent, and the diffraction peaks of the lithiated compounds LiC_{12} (~11.58°) and LiC_6 (~11.08°) are distinguishable. The transitions from the dilution stage to LiC_{12} and then to LiC_6 are very evident. When the intensity of the LiC_{12} diffraction peak reaches its maximum at about 50% lithium concentration, LiC_6 begins to form and the LiC_{12} peak begins to decrease.

The volume expansion due to Li^+ intercalation results in changes in both interlayer and intralayer distances of graphite. The interlayer spacing of graphite can be calculated using Bragg's equation $2d\sin\theta = n\lambda$, as shown in Figure 8B. The calculated interlayer distances correspond to the graphite (002) peak [Figure 8A], increasing from 3.35 to 3.70 Å. The interlayer spacing of graphite rapidly increases from 0% to 38% SOC, remains almost unchanged from 38% to 78% SOC, and linearly grows from 78% to 100% SOC. These results align with the established experimental findings[44,50]. Moreover, this finding clarifies the unchanged partial molar volume observed at 40% SOC in previous studies, further corroborating the current results[45].

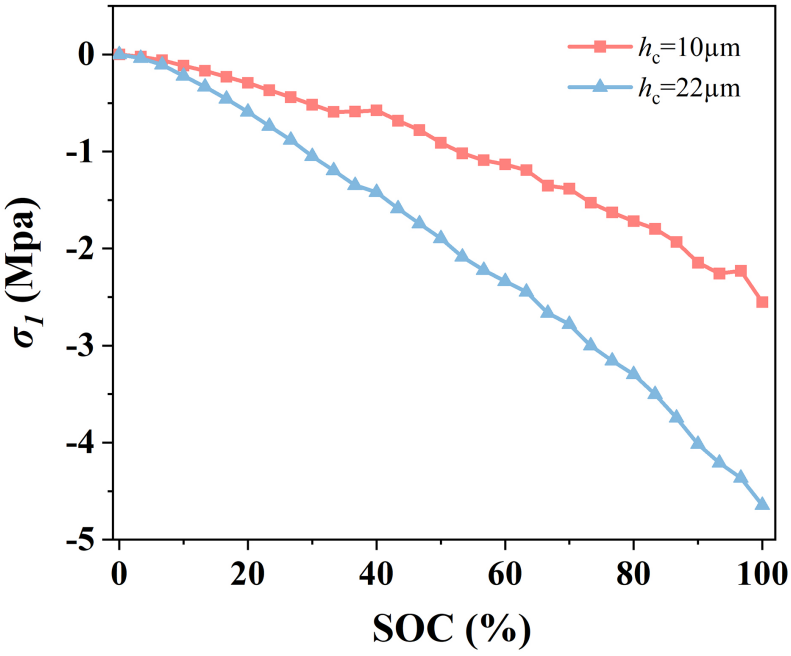

Figure 7. The stress of graphite composite electrode (h_a = 40 μm) at the third cycle.

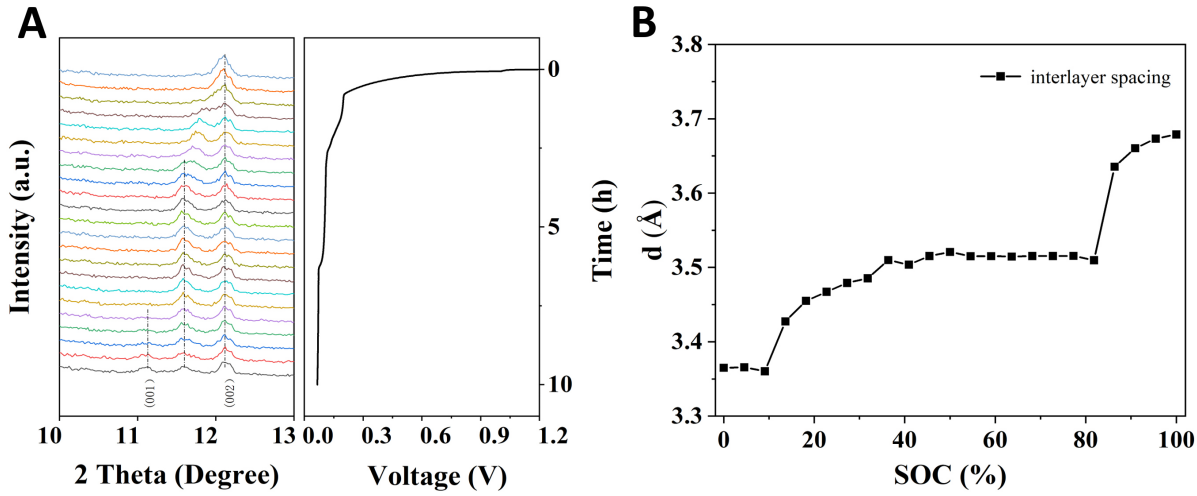

Figure 8. (A) *In-situ* XRD diffraction spectroscopy and (B) interlayer spacing.

The calculated spacing exhibits an almost linear relationship. Combined with the XRD diffraction patterns and the voltage plateaus in Figure 5, three stages can be identified. As shown in Figure 9, three stages were identified by combining XRD diffraction patterns with voltage plateaus in Figure 5. The first stage, the formation of LiC_{12} from C, showed a shift of the diffraction peak towards lower 2θ values, indicating an increase in interlayer spacing and partial molar volume. In the intermediate stage, the transition from liquid stage 2L to solid stage 2 (LiC_{12}) did not result in a shift in the diffraction peak position, creating a plateau and maintaining a constant partial molar volume. In the third stage, the transition from LiC_{12} to LiC_6 led to volume changes due to the coexistence of the 002 and 001 phases, resulting in an increase in partial molar volume.

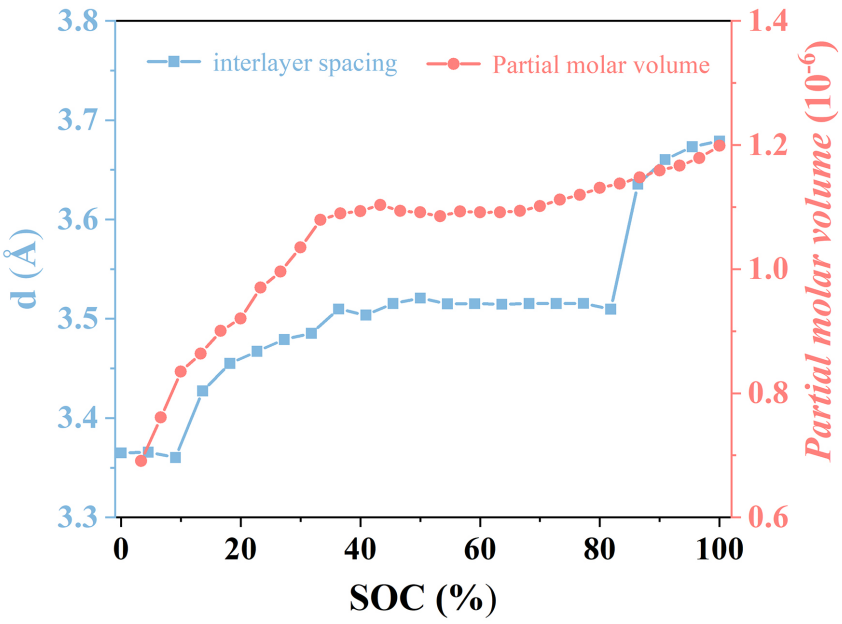

Figure 9. Graphite composite electrode third cycle partial molar volume and layer spacing comparison.

These changes in partial molar volume corresponded precisely to the observed phase transitions. Through *in situ* XRD testing, the study accurately determined and verified the partial molar volume of graphite composite electrodes during electrochemical cycling. The XRD results supported the partial molar volume measurements, providing further insights into the lithium intercalation mechanism in graphite anodes and the volumetric changes of the active material.

CONCLUSIONS

Combining the *in-situ* XRD and curvature testing, the electrochemical-mechanical coupling characteristics have been elucidated in graphite composite electrodes. The research has demonstrated that both Young's modulus and partial molar volume of lithiated graphite electrodes increase with the degree of lithiation. Initially, Young's modulus rises rapidly, then more gradually, ultimately reaching 0.97 GPa. At SOC 0% to 30%, the partial molar volume increases linearly from 0.69×10^{-6} to 1.07×10^{-6}. Between 30% and 68% SOC, the partial molar volume shows a plateau with slow growth, and from 68% to 100% SOC, it rises from 1.1×10^{-6} to 1.21×10^{-6}. XRD measurements indicate three distinct stages in the change of graphite interlayer spacing: an initial increase from 3.35 to 3.5 Å, a plateau at 3.5 Å, followed by a further increase to 3.70 Å upon full lithiation. The research demonstrates an increase in elastic modulus during the lithiation process, as well as staged changes in partial molar volume attributed to phase transitions. The developed methodology in this study provides valuable insights into the mechanism of lithium intercalation and volume change patterns in graphite anodes. These results enhance our understanding of multi-scale mechano-electro-chemical mechanisms, providing a foundation for addressing degradation and optimizing the performance and efficiency of lithium-ion batteries.

DECLARATIONS

Author contributions

Research design and writing-original draft: Li, D.; Liu, J.; Shen, C.
Data collection and experiment: Liu, J.; Gu, H.

Data collection and analysis: Liu, J.; Yao, Y.
Review and editing: Li, D.; Jiang, H.; Shen, K.
Refining the ideas and finalizing this paper: Li, D.; Zheng, Y.

Availability of data and materials

The data can be shared upon request when our program is finished.

Financial support and sponsorship

This work was funded by the National Natural Science Foundation of China (Grant Nos. 12102264).

Conflicts of interest

All authors declared that there are no conflicts of interest.

Ethical approval and consent to participate

Not applicable.

Consent for publication

Not applicable.

REFERENCES

1. Chen, S.; Dai, F.; Cai, M. Opportunities and challenges of high-energy lithium metal batteries for electric vehicle applications. *ACS. Energy. Lett.* **2020**, *5*, 3140-51. DOI
2. Du, S.; Gao, F.; Nie, Z.; Liu, Y.; Sun, B.; Gong, X. Assessing resource depletion of NCM lithium-ion battery production for electric vehicles: an exergy-based perspective. *J. Clean. Prod.* **2023**, *420*, 138415. DOI
3. Dai, L.; Li, B.; Li, J.; Xu, Z. Preparation of high-performance manganese-based pseudocapacitor material by using spent lithium-ion battery anode graphite via mechanochemical pretreatment. *Carb. Neutral.* **2024**, *3*, 79. DOI
4. Zhang, H.; Song, Z.; Fang, J.; et al. Electrolyte optimization for graphite anodes toward fast charging. *J. Phys. Chem. C.* **2023**, *127*, 2755-65. DOI
5. Luo, P.; Zheng, C.; He, J.; et al. Structural engineering in graphite-based metal-ion batteries. *Adv. Funct. Mater.* **2022**, *32*, 2107277. DOI
6. Yang, X.; Wen, H.; Lin, Y.; et al. Emerging research needs for characterizing the risks of global lithium pollution under carbon neutrality strategies. *Environ. Sci. Technol.* **2023**, *57*, 5103-6. DOI
7. Yang, B.; Tamirat, A. G.; Bin, D.; Yao, Y.; Lu, H.; Xia, Y. Regulating intercalation of layered compounds for electrochemical energy storage and electrocatalysis. *Adv. Funct. Mater.* **2021**, *31*, 2104543. DOI
8. Laipan, M.; Xiang, L.; Yu, J.; et al. Layered intercalation compounds: mechanisms, new methodologies, and advanced applications. *Prog. Mater. Sci.* **2020**, *109*, 100631. DOI
9. Li, Y.; Yan, H.; Xu, B.; Zhen, L.; Xu, C. Y. Electrochemical intercalation in atomically thin van der waals materials for structural phase transition and device applications. *Adv. Mater.* **2021**, *33*, e2000581. DOI
10. Khan, F. M. N. U.; Rasul, M. G.; Sayem, A.; Mandal, N. K. Design and optimization of lithium-ion battery as an efficient energy storage device for electric vehicles: a comprehensive review. *J. Energy. Storage.* **2023**, *71*, 108033. DOI
11. Zhang, S.; Zhao, K.; Zhu, T.; Li, J. Electrochemomechanical degradation of high-capacity battery electrode materials. *Prog. Mater. Sci.* **2017**, *89*, 479-521. DOI
12. Li, L.; Qin, R.; Zhan, R.; et al. Modification with graphite and sulfurized amorphous carbon for high-performance silicon anodes in lithium-ion batteries. *J. Energy. Storage.* **2024**, *98*, 113196. DOI
13. Banerjee, J.; Dutta, K. Materials for electrodes of Li-ion batteries: issues related to stress development. *Crit. Rev. Solid. State. Mater. Sci.* **2017**, *42*, 218-38. DOI
14. Ezeigwe, E. R.; Dong, L.; Manjunatha, R.; Tan, M.; Yan, W.; Zhang, J. A review of self-healing electrode and electrolyte materials and their mitigating degradation of Lithium batteries. *Nano. Energy.* **2021**, *84*, 105907. DOI
15. Zeng, C.; Liang, J.; Cui, C.; Zhai, T.; Li, H. Dynamic investigation of battery materials via advanced visualization: from particle, electrode to cell level. *Adv. Mater.* **2022**, *34*, e2200777. DOI
16. Yang, W.; Xie, H.; Shi, B.; Song, H.; Qiu, W.; Zhang, Q. In-situ experimental measurements of lithium concentration distribution and

strain field of graphite electrodes during electrochemical process. *J. Power. Sources.* **2019**, *423*, 174-82. DOI

17. Liu, D.; Shadike, Z.; Lin, R.; et al. Review of recent development of in situ/operando characterization techniques for lithium battery research. *Adv. Mater.* **2019**, *31*, e1806620. DOI
18. Li, T.; Panda, P. K.; Hsieh, C.; Gandomi, Y. A.; Yang, P. Lithium iron phosphate cathode supported solid lithium batteries with dual composite solid electrolytes enabling high energy density and stable cyclability. *J. Energy. Storage.* **2024**, *81*, 110444. DOI
19. Xiong, T.; Zhang, D.; Yeo, J. Y.; et al. Interfacial design towards stable zinc metal-free zinc-ion batteries with high energy density. *J. Mater. Chem. A.* **2024**, *12*, 5499-507. DOI
20. Jangid, M. K.; Mukhopadhyay, A. Real-time monitoring of stress development during electrochemical cycling of electrode materials for Li-ion batteries: overview and perspectives. *J. Mater. Chem. A.* **2019**, *7*, 23679-726. DOI
21. Xie, H.; Song, H.; Guo, J.; Kang, Y.; Yang, W.; Zhang, Q. In situ measurement of rate-dependent strain/stress evolution and mechanism exploration in graphene electrodes during electrochemical process. *Carbon* **2019**, *144*, 342-50. DOI
22. Sauerteig, D.; Ivanov, S.; Reinshagen, H.; Bund, A. Reversible and irreversible dilation of lithium-ion battery electrodes investigated by in-situ dilatometry. *J. Power. Sources.* **2017**, *342*, 939-46. DOI
23. de, V. L. S.; Xu, R.; Xu, Z.; et al. Chemomechanics of rechargeable batteries: status, theories, and perspectives. *Chem. Rev.* **2022**, *122*, 13043-107. DOI
24. Wang, B.; Le, F. L. W.; Brookfield, A.; McInnes, E. J. L.; Dryfe, R. A. W. Resolution of lithium deposition versus intercalation of graphite anodes in lithium ion batteries: an in situ electron paramagnetic resonance study. *Angew. Chem. Int. Ed.* **2021**, *60*, 21860-7. DOI PubMed PMC
25. Shi, B.; Kang, Y.; Xie, H.; Song, H.; Zhang, Q. In situ measurement and experimental analysis of lithium mass transport in graphite electrodes. *Electrochim. Acta.* **2018**, *284*, 142-8. DOI
26. Jones, E. M. C.; Silberstein, M. N.; White, S. R.; Sottos, N. R. In situ measurements of strains in composite battery electrodes during electrochemical cycling. *Exp. Mech.* **2014**, *54*, 971-85. DOI
27. Dahn, J. R. Phase diagram of Li_xC_6. *Phys. Rev. B. Condens. Matter.* **1991**, *44*, 9170-7. DOI PubMed
28. Lăcătușu, M. E.; Theil, K. L. E.; Johnsen, R. K. M.; et al. A multimodal operando neutron study of the phase evolution in a graphite electrode. *Arxiv* **2021**, 03564. DOI
29. Qiu, S.; Xiao, L.; Sushko, M. L.; et al. Manipulating adsorption-insertion mechanisms in nanostructured carbon materials for high-efficiency sodium ion storage. *Adv. Energy. Mater.* **2017**, *7*, 1700403. DOI
30. Park, J. H.; Yoon, H.; Cho, Y.; Yoo, C. Y. Investigation of lithium ion diffusion of graphite anode by the galvanostatic intermittent titration technique. *Materials* **2021**, *14*, 4683. DOI PubMed PMC
31. Oka, H.; Makimura, Y.; Uyama, T.; Nonaka, T.; Kondo, Y.; Okuda, C. Changes in the stage structure of Li-intercalated graphite electrode at elevated temperatures. *J. Power. Sources.* **2021**, *482*, 228926. DOI
32. Dimiev, A. M.; Shukhina, K.; Behabtu, N.; Pasquali, M.; Tour, J. M. Stage transitions in graphite intercalation compounds: role of the graphite structure. *J. Phys. Chem. C.* **2019**, *123*, 19246-53. DOI
33. He, Y.; Hu, H.; Song, Y.; Guo, Z.; Liu, C.; Zhang, J. Effects of concentration-dependent elastic modulus on the diffusion of lithium ions and diffusion induced stress in layered battery electrodes. *J. Power. Sources.* **2014**, *248*, 517-23. DOI
34. Chiuhuang, C.; Huang, H. S. Critical lithiation for C-rate dependent mechanical stresses in $LiFePO_4$. *J. Solid. State. Electrochem.* **2015**, *19*, 2245-53. DOI
35. Zhao, H.; Zhang, W.; Zheng, K.; Xu, W. A novel high-efficient lithium-ion battery serial formation system scheme based on partial power conversion. *J. Energy. Storage.* **2024**, *97*, 112350. DOI
36. Yu, W.; Deng, N.; Feng, Y.; et al. Understanding multi-scale ion-transport in solid-state lithium batteries. *eScience* **2025**, *5*, 100278. DOI
37. Jiang, M.; Ammigan, K.; Lolov, G.; Pellemoine, F.; Liu, D. A novel method for quantifying irradiation damage in nuclear graphite using Raman spectroscopy. *Carbon* **2023**, *213*, 118181. DOI
38. de Araujo L, Sarou-Kanian V, Sicsic D, Deschamps M, Salager E. Operando nuclear magnetic resonance spectroscopy: detection of the onset of metallic lithium deposition on graphite at low temperature and fast charge in a full Li-ion battery. *J. Magn. Reson.* **2023**, *354*, 107527. DOI
39. Li, J.; Qin, Y.; Shen, J.; Chen, Y. Evolution of carbon nanostructures during coal graphitization: insights from X-ray diffraction and high-resolution transmission electron microscopy. *Energy* **2024**, *290*, 130316. DOI
40. An, J.; Shi, L.; Chen, G.; Li, M.; Liu, H.; Yuan, S.; Chen, S.; Zhang, D. Insights into the stable layered structure of a Li-rich cathode material for lithium-ion batteries. *J. Mater. Chem. A.* **2017**, *5*, 19738-44. DOI
41. Cui, S.; Wang, Y.; Liu, S.; Li, G.; Gao, X. Evolution mechanism of phase transformation of Li-rich cathode materials in cycling. *Electrochim. Acta.* **2019**, *328*, 135109. DOI
42. Nonaka, T.; Kawaura, H.; Makimura, Y.; Nishimura, Y. F.; Dohmae, K. In situ X-ray Raman scattering spectroscopy of a graphite electrode for lithium-ion batteries. *J. Power. Sources.* **2019**, *419*, 203-7. DOI
43. Schweidler, S.; de, B. L.; Schiele, A.; Hartmann, P.; Brezesinski, T.; Janek, J. Volume changes of graphite anodes revisited: a combined *operando* X-ray diffraction and *in situ* pressure analysis study. *J. Phys. Chem. C.* **2018**, *122*, 8829-35. DOI
44. Park, J.; Park, S. S.; Won, Y. S. In situ XRD study of the structural changes of graphite anodes mixed with SiO_x during lithium insertion and extraction in lithium ion batteries. *Electrochim. Acta.* **2013**, *107*, 467-72. DOI
45. Li, D.; Wang, Y.; Lu, B.; Zhang, J. Real-time measurements of electro-mechanical coupled deformation and mechanical properties of

commercial graphite electrodes. *Carbon* **2020**, *169*, 258-63. DOI

46. Weisenberger, C.; Harrison, D. K.; Zhou, C.; Knoblauch, V. Revealing the effects of microstructural changes of graphite anodes during cycling on their lithium intercalation kinetics utilizing operando XRD. *Electrochim. Acta.* **2023**, *461*, 142629. DOI
47. Li, B.; Chao, Y.; Li, M.; et al. A review of solid electrolyte interphase (SEI) and dendrite formation in lithium batteries. *Electrochem. Energy. Rev.* **2023**, *6*, 147. DOI
48. Li, D.; Wang, Y. In-situ measurements of mechanical property and stress evolution of commercial graphite electrode. *Mater. Des.* **2020**, *194*, 108887. DOI
49. Xiong, Y.; Liu, Y.; Chen, L.; et al. New insight on graphite anode degradation induced by Li-plating. *Energy. Environ. Mater.* **2022**, *5*, 872-6. DOI
50. Knorr, J.; Gomez-Martin, A.; Hsiao, H.; Adam, A.; Rödl, B.; Danzer, M. A. Effect of different charge rates on the active material lithiation of Gr/SiOx blend anodes in lithium-ion cells. *J. Energy. Storage.* **2024**, *86*, 111151. DOI